Crimson Publishers
Wings to the Research

Research Article

Long Term Tracking Nanoparticles Composites for Bone Tissue Regeneration: Insights

Rodrigo Osorio-Arciniega[1], Manuel García-Hipólito[2], Octavio Alvarez-Fregoso[2] and Marco Antonio Alvarez-Perez[1]

[1]Tissue Bioengineering Laboratory, Faculty of Dentistry, Mexico

[2]Institute for Materials Research, Mexico

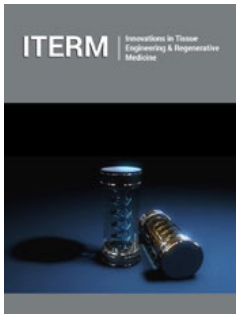

***Corresponding author:** Rodrigo Osorio-Arciniega, Faculty of Dentistry, DEPeI, National Autonomous University, Circuito Exterior s/n. Cd. Universitaria, Coyoacán 04510, Mexico

Submission: May 05, 2023
Published: June 07, 2023
Volume 2 - Issue 1

How to cite this article: Rodrigo Osorio-Arciniega, Manuel García-Hipólito, Octavio Alvarez-Fregoso and Marco Antonio Alvarez-Perez. Long Term Tracking Nanoparticles Composites for Bone Tissue Regeneration: Insights. Innovations Tissue Eng Regen Med. 2(1).ITERM.000527.2023.

Abstract

Given the intricate physiological processes involved, creating bone grafts or prosthetic implants for clinical use can be challenging. Fortunately, recent advancements in nanotechnology have accelerated and facilitated the development of functional bone grafts and implants. Rare Earth (RE) materials are a class of emerging biomaterials that possess unique properties such as biocompatibility, fluorescence upconversion, and anti-inflammatory effects, making them highly valuable in tissue engineering. Recently, there has been an increasing need for materials that can enhance tissue regeneration and advance our knowledge of bone restoration over extended periods of time. This study offers a novel technique for creating tunable green and yellow upconversion composite emissions by embedding lanthanide nanoparticles YAG:Ce^{3+} in Poly(Vinyl Alcohol) (PVA) scaffolds and stimulating them with 400nm blue wavelength light. By combining upconversion lanthanide nanoparticles with image superposition methodology, we are able to reliably track implanted materials or scaffolds over time during long-term fluorescence surveillance. This novel approach provides an effective way to distinguish between different materials and monitor their behavior *in vitro* and *in vivo*.

Keywords: Rare earth materials; Upconversion; Composite; Long-Term fluorescence; Poly(Vinyl Alcohol) (PVA)

Introduction

Rare-earth elements, also known as rare-earth metals, are a group of seventeen chemical elements located in the periodic table. This group includes fifteen lanthanides and two additional elements, scandium and yttrium. The International Union of Pure and Applied Chemistry (IUPAC) defines this group of elements as rare-earth elements due to their limited abundance in the earth's crust. Additionally, these elements exhibit similar chemical properties, which makes it difficult to separate them from each other [1]. REE elements typically exist as trivalent cations and have a configuration of ([Xe]4fn 5s2 5p6 [n=0-14]). The 4f and 5p electrons are protected by the outer 5s, therefore environmental factors have little impact on their transitions.

Due to photoluminescence, this enables RE materials to have distinctive spectroscopic characteristics such long-lasting emission, narrow bandwidth, and bright fluorescent emissions [2]. Additionally, there is an observed phenomenon in lanthanide ions known as the "lanthanide contraction," which results in a gradual reduction in the ionic radius from La^{3+} (1.06Å) to Lu^{3+} (0.85Å) [1]. Usually, photoluminescence abides by Stokes' law, which states that the luminescence's wavelength must be longer than the stimulating radiation's wavelength. As a result, RE nanoparticles (1-100nm) are becoming crucial for new tissue engineering applications and biomedical imaging due to their ability to reduce

autofluorescence and their ability to penetrate biological tissues [2]. Upconversion materials, mainly based on $NaYF_4$, $NaYbF_4$, and LaPO matrices, have been used in small-animal imaging and long-term real-time cell imaging [3]. Few reports of lanthanide co-doped polymer scaffolds for upconversion luminescence have been made. Furthermore, there are no reports on the use of upconversion material for accurately labeling implanted material and tracking material-tissue interactions at this time. This study suggests a new technique for marking implanted material and precisely tracking material-tissue interactions: lanthanide co-doped PVA scaffolds with stable upconversion luminescence and bone-bonding capacity [3].

PVA is a water-soluble polymer that has received FDA approval and is noted for its simple synthesis process, biocompatibility, and biodegradability. It is made by polymerizing vinyl acetate and alcoholizing it under alkaline or acidic catalysis [4]. YAG:Ce^{3+} is an excellent candidate for biological applications due to its intense blue light absorption, sprightly yellow emission with a high quantum yield, and outstanding stability at high temperatures [5]. To enhance their luminous qualities, YAG: Ce^{3+} phosphors were made using the sol-gel method and sintered at a certain temperature for two and six hours. In order to develop a tracking cell bone regeneration scaffold for upcoming *in vitro* and *in vivo* tests, these nanophosphors were then incorporated into a PVA scaffold.

Materials and Methods

Luminescent upconversion nanocrystals synthesis

Sol-gel technique was used to carry out the synthesis. The reagents utilized in this study included Y $(NO_3)3{\cdot}6H_2O$, $Al(NO_3)3{\cdot}6H_2O$, $Ce(NO_3)3{\cdot}6H_2O$, and $C_4H_6O_6$, all of which were procured from Sigma-Aldrich® with a purity of 99.99%. In a 1:2 ratio, tartaric acid ($C_4H_6O_6$) was used as the precursor agent. Ce^{3+} ions were presented in concentrations percentages of 3%. Prior to dispersion in deionized water, which had been previously filtered on a 0.2µm nylon membrane, the reagents were subjected to rigorous magnetic stirring for 20-24 hours. In order to better regulate the temperature, the mixture was then heated to 80 °C for three hours while being continuously stirred in a spray pyrolysis rack. The aggregates were collected and underwent a thermal-annealing treatment, whereby they were raised to 1100 °C using a Felisa FE-290 oven for 2 and 6 hours. Finally, all aggregates underwent a grinding treatment using an Agate mortar and pestle.

Luminescent fibrillar spun composites synthesis

Poly(Vinyl Alcohol) (PVA) pellets called Ingeo 2003D, with a molecular weight of 192,000 ($C_3H_6O_3$), were purchased from Promaplast in Mexico. Chloroform ($CHCl_3$) and ethyl alcohol absolute anhydrous (CH_3CH_2OH), were provided by J.T. Baker and utilized without additional purification. Polymeric solutions of PVA were used to synthesize composite fibrillar scaffolds through the Air Jet Spraying (AJS) technique. First, 10wt% polymer solutions were prepared by dissolving PLA pellets in chloroform and stirring for 24 hours. Afterwards, ethanol (70%) was added to the mixture and stirred for an additional 15 minutes until a uniform solution was achieved. The volume ratio of chloroform to ethanol used in the process was 3:1.Luminescent nanophosphor YAG:Ce^{3+}, was added to the polymer solutions. Prior to synthesis, the solutions were sonicated for 2 hours to ensure homogenization of the nanophosphor using a Branson brand ultrasonic bath. The polymer solution was then placed in an ADIR model 699 airbrush with a 0.3mm diameter nozzle, with a gravitational feed used to synthesize the scaffolds. The airbrush was connected to a pressurized argon tank (CAS number 7740-37, concentration >99%, PRAXAIR México, Nuevo León, México), and a constant pressure of 25 psi was maintained at a gap of 10cm between the nozzle and the target. High-quality fibers were deposited as a result of the adjusted settings.

Luminescent nanocrystals characterization techniques X-Ray Diffraction Analysis (XRD)

The crystal phase of Ce^{3+} doped $Y_3Al5O12$ nanocrystals was analyzed using a Phillips X'pert X-ray diffractometer with a Cu source and Kα1 radiation (λ= 0.15406 nm), scanned over a 2θ range of 20-80°. The Scherrer equation was used to calculate the average crystallite size from the broadening of the XRD peaks:

$$D= 0.9\lambda/\beta\theta$$

Where 0.9 is a constant that depends on the shape of the crystallite (0.9×57.3), is the XRD wavelength, is the corrected half-width of the strongest diffraction peak, and is the diffraction angle.

Scanning Electron Microscopy (SEM)

To examine the surface of the luminescent nanophosphor YAG:Ce^{3+}, SEM was utilized with a JEOL JSM-5300 equipment. The samples were carefully deposited on conductive carbon tape prior to being exposed to a beam of accelerated electrons, which were used to sweep the surface of the sample.

Photoluminescence (PL) analyses

The present study conducted Photoluminescence (PL) analyses to investigate the excitation and emission spectra of diverse synthesized luminescent nanocrystals. A Hitachi F-7000 spectrophotometer equipped with a xenon arc lamp was utilized to examine the samples. The excitation wavelength of 450nm, was selected owing to its highest PL emission intensity

Cell culture

Human Fetal Osteoblasts (hFOB), ATTC cell line number 1.19, were cultured and expanded in DMEM culture medium supplemented with 10% Fetal Bovine Serum (FBS), an antibiotic solution (penicillin 100UI/ml), streptomycin (100µg/ml), and fungizone (0.3µg/ml). The cultures were maintained at a temperature of 37 °C, in an atmosphere of 95% air and 5% CO_2 in an environment with 100% humidity.

Cell interaction with composite scaffolds

To observe the interaction between hFOB cells and composite fibrous scaffolds, we seeded 1x104 cells/mL and incubated them

for 24 hours. Next, we fixed them with 4% PFA for 15 minutes and observed them using fluorescence microscopy with an Axio Imager A2 Zeiss. We maintained standard culture conditions during incubation and performed a PBS wash between each step to remove non-adherent cells from the composite scaffold. Images were analyzed in AmScope Optic Microscopy equipment (excitation=400nm wavelength).

Design of the *in vivo* study and subcutaneous placement of implants

Ethical approval was granted by the Institutional Research, Ethical, and Animal Care and Use Committee of the Faculty of Dentistry at the National Autonomous University of Mexico (UNAM) for all animal procedures conducted in this study.

Implantation of scaffolds in animals involved twelve adult male Wistar rats, each weighing 200g and aged 12 weeks. These rats were randomly assigned to four study groups, with three rats per scaffold unit. The rats were obtained from the vivarium of the Medical Faculty at UNAM. Each group underwent subcutaneous implantation of two scaffolds (bare PLA and YAG:Ce_{3+}/PVA) for two different time points, specifically 2 and 4 weeks. Under general anesthesia (Ketamine 80mg/kg and Xylazine 10mg/kg), all animal groups underwent surgical implantation of the scaffolds. Prior to scaffold placement, the surgical site was prepared by shaving and cleaning with a disinfectant. A rectangular flap of approximately 2x1cm was created: one on the upper right side for the placement of the 10% w/v PVA scaffold as the control, and one on the left side for the YAG:Ce^{3+}/PVA scaffold. Each scaffold was sutured to the dermis using 5-0 Nylon sutures to ensure stability and prevent displacement. The animals were housed in specially designed rooms with a temperature of 18-22 °C and a relative humidity of 50%, following a 12-hour light-dark cycle. They had unrestricted access to water and a standard laboratory diet. Post-surgical monitoring was conducted to assess the animals' general condition, wound appearance, bleeding, exudate, and scaffold integrity.

Histological analysis

Histological analyses were performed to examine the tissue-biomaterial interactions within the implantation sites of the scaffolds and their surrounding tissue. A Leica Microscope (Microsystems, NY, USA) was used for this purpose. The animals were euthanized at two different time points (2 and 4 weeks) using a CO_2 chamber. The scaffolds, along with the surrounding soft tissue, were carefully dissected from the rats. Subsequently, the samples were fixed in formalin and stained with Hematoxylin and Eosin (H&E) to assess the inflammatory response.

Statistical analysis

Statistical analysis was performed to analyze the quantitative data, presented as mean±standard deviation. An analysis of variance (ANOVA) was conducted using GraphPad Prism 6.0c software (GraphPad Software Inc., La Jolla, USA) to compare the data among the study groups. Statistical significance was determined with p-values less than 0.05 (*p≤0.05) considered significant, p-values less than 0.01 (**p≤0.01) considered highly significant, and p-values less than 0.001 (***p≤0.001) also considered highly significant.

Result and Discussion

YAG:Ce3+ nanophosphors precursors were synthesized through an driven sol–gel technique [6]. The lanthanide powder mixture was created by a series of procedures including: rigorous magnetic agitation, evaporation of organic elements, grinding, sieving, and sintered at 1100 °C for varying durations of 2 and 6 hours. The shape of the YAG:Ce^{3+} nanophosphorus was depicted in (Figure 1A & 1B), which showed that the powder combination was dispersed in a heterogeneous manner. Agglomeration between particles is what causes the asymmetrical forms with a quasispherical tendency. This suggests a high-density nanophosphorus storage system with other possible flaws [7]. In Figure 2A, the $Y_{2.97}Al_5O_{12:0.03}Ce^{3+}$ nanophosphorus excitation and emission spectra after two and six hours of heat treatment at 1100 °C temperature are shown.

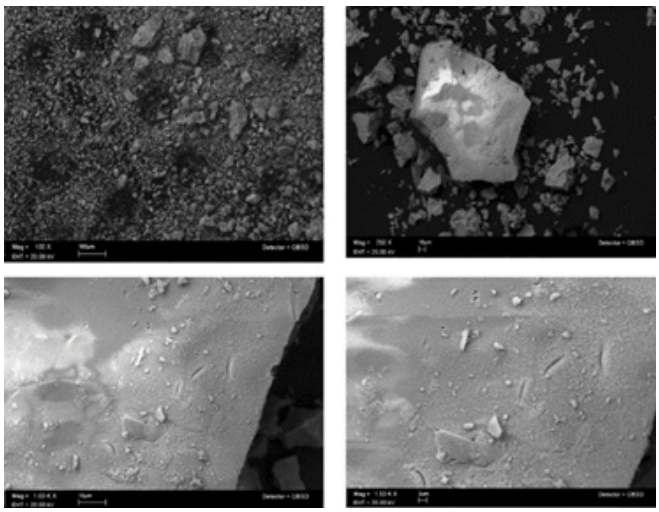

Figure 1: SEM images of YAG: Ce^{3+} nanophosphors, showing their morphologies at 100μ , 10μ, and 2μ, as shown in (a-d), respectively.

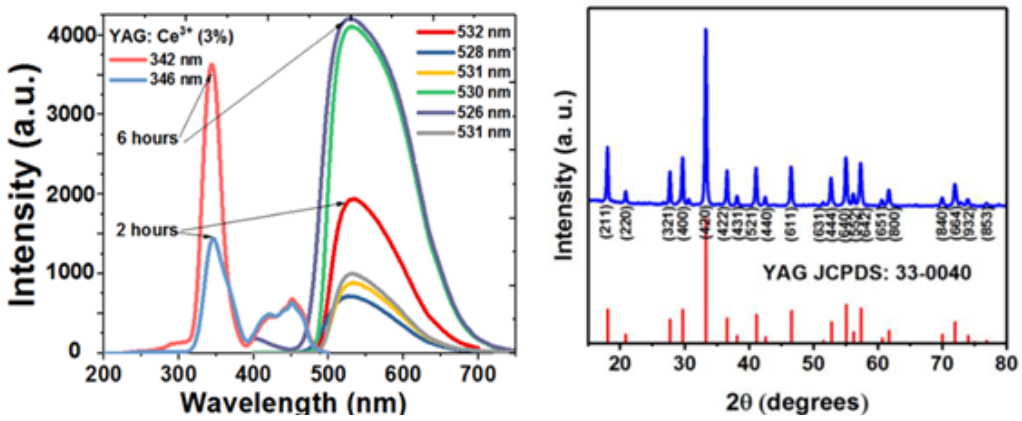

Figure 2: a) Upconversion luminescence spectra and fluorescent images obtained at an excitation wavelength of 450nm and an emission wavelength of 540nm compared at different times (2 and 6 hours) of annealing treatment and, b) X-Ray Diffraction (XRD) patterns compared with 33-0040 crystallographic data sheet.

The excitation spectrum of the nanophosphorus was broad, spanning 400 to 500nm, which is exactly in line with the blue light emission spectrum of GaN LED chips (450-480nm). The Ce^{3+} ions' electron 4f1-5d1 transition is what is responsible for the intense yellow emission at 550nm after being excited at 460nm. The broad band emission spectra recorded at 550nm showed that the crystal field strength and symmetry of the host lattice had a substantial impact on the luminescent characteristics of the Ce^{3+} ions. Interestingly, we also saw that the luminous characteristics of the dopant ion enhanced due to better dopant ion embedding in the crystal lattice [8].

Figure 2b shows the XRD patterns of the $Y_{2.97}Al_5O_{12:0.03}Ce^{3+}$ (x=3%) nanophosphors that were heated for 6 hours at a fixed temperature. The heat-treated nanophosphors had discrete peaks that were in agreement with the cubic $Y_3Al_5O_{12}$ PDF crystallographic card (33-0040). As the heat-treated temperature increased, shorter full-width at half maximums and sharper peaks were observed, indicating that $Y_{2.97}Al_5O_{12:0.03}Ce^{3+}$ (x=3%) nanophosphors treated at higher temperatures have greater crystallinity [9]. The average crystal sizes were estimated using Scherrer's equation, with values of 52 and 65nm obtained for samples calcined at 1100 °C for 2 and 6 hours, respectively [10]. As the concentration of Ce^{3+} ion dopants was maintained at 3%, it was found that the luminosity of the $Y_{2.97}Al_5O_{12}$:0.03Ce^{3+} nanophosphors increased. However, the emission intensity steadily declined as the dopant concentration was raised further. Luminescence concentration quenching, which is brought on by energy transfer between nearby luminescence centers and occurs at high dopant concentrations, could be utilized to explain this phenomenon [11].

By incorporating the luminous nanophosphors in PVA using the Air Jet Spraying method (AJS), we were able to produce a traceable scaffold. Both the PVA and PVA/YAG:Ce^{3+} scaffolds were shown to have a porous interconnected-like structure in (Figure 3A & 3B). The coordinated porosity structure of PVA/YAG:Ce^{3+} scaffolds was preserved despite the addition of a modest amount of nanophosphors, indicating that PVA's porous capabilities were unaffected [12]. The average pore size of PVA was 226.8nm, while the average pore size of PVA that had been modified with nanophosphors was 264.1nm [PVA/YAG:Ce_{3+} (3%)]. The microstructure of luminescent composite scaffolds was examined by SEM, as shown in Figure 4(a-c). The results showed that the roughness of the scaffolds increased when nanophosphors were added to PVA. In PVA/YAG:Ce^{3+} (3%), the nanophosphors were not dispersed uniformly, and agglomerated particles were seen on the fibril, indicating that polymer beads were conjugating with YAG:Ce^{3+} nanophosphors [12].

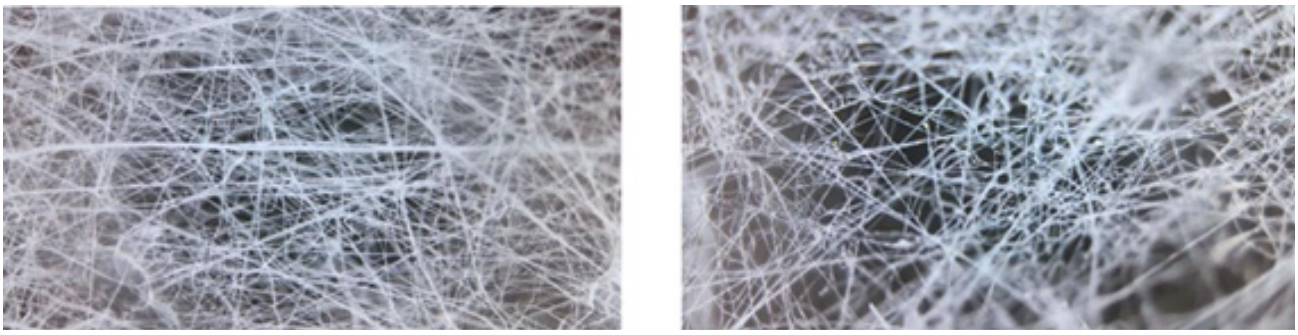

Figure 3: a) Optic micrograph of the PVA scaffold, exhibiting porous interconnection, and b) PVA polymer combined with embedded YAG:Ce^{3+} nanophosphor.

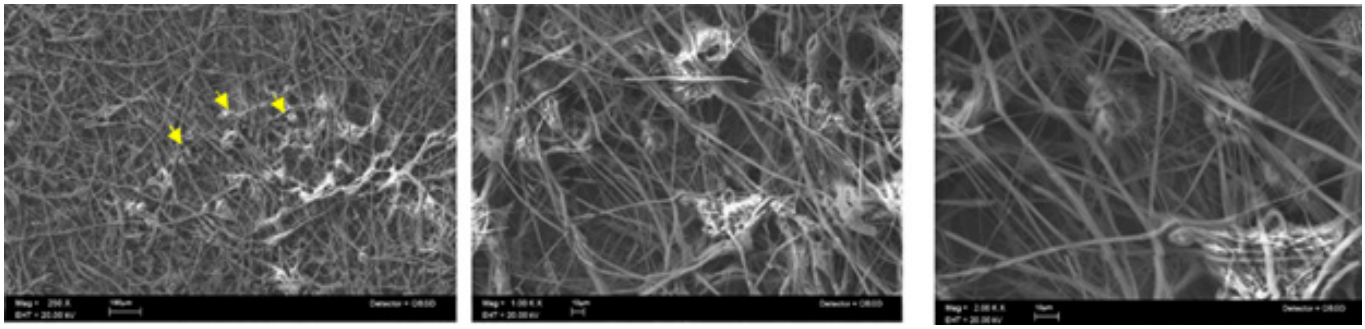

Figure 4: (a-c) SEM images of YAG: Ce^{3+} conjugated scaffold, demonstrating dispersion, roughness, and interconnection of the biomaterials.

The PVA scaffold holds great promise as a material for bioregeneration. The nanophosphors embedded in the fibrils were analyzed using a photoluminescent technique, owing to their unique luminescent properties. In this study, we excited the biomaterial with a 450nm wavelength, which resulted in a natural emission at 540nm. The composites exhibited a highly luminescent yellow emission, providing a robust local tracking capability across the length of the scaffold. Furthermore, we filtered the incident irradiation to highlight the noble properties of the embedded nanophosphors, thereby eliminating the PVA autofluorescence, Figure 5. This test also allows us to trace the brightness of the nanophosphors and assess their distribution. The scaffold additionally made it possible to spot pores, struts, and vacant areas in the cross-sectional field. The surface of the fibers displays a rough texture with noticeable pores. The inclusion of beads within the fiber structure suggests that capillary instability was induced during fiber spraying, with the dominant factor being the viscoelasticity of the polymer solutions and the use of volatile organic solvents during AJS synthesis [13]. Several studies have investigated how adjusting electrospinning parameters can affect scaffold production. By altering the synthesis of scaffolds, it is possible to achieve favorable modifications in their structures and mechanical properties. This, in turn, promotes the production of extracellular proteins by cells, resulting in tissue that is suitable for implantation. Post-production techniques such as sterilization can further enhance the desired features of the scaffolds. However, it is crucial to consider that these processes can also influence the mechanical properties of the scaffolds.

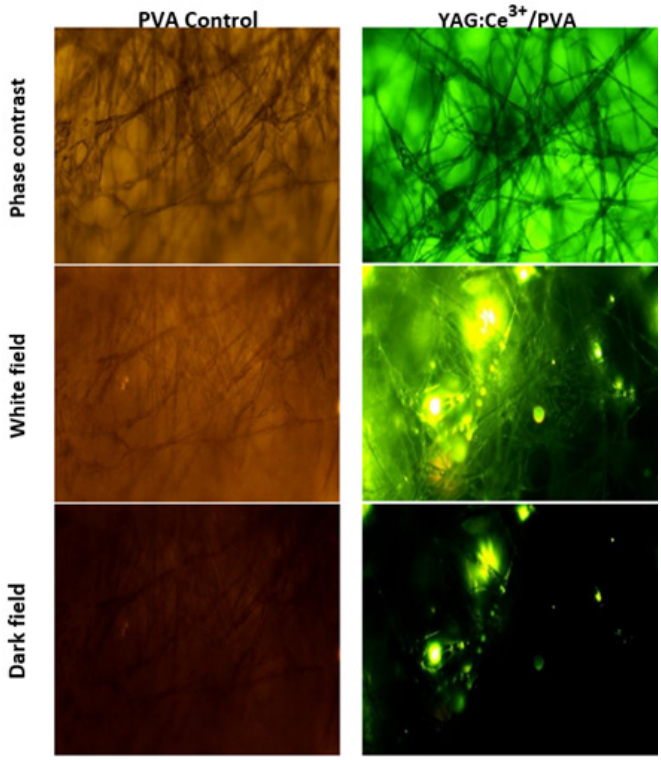

Figure 5: Luminescence of PVA and PVA/YAG: Ce^{3+} scaffolds observed under optical microscopy. (a) Bright-field, (b) dark-field, and (c) phase-contrast images of the scaffolds with a scale bar of 20μm. The luminescence of the scaffolds is due to the emission of the embedded YAG: Ce^{3+} nanophosphors.

In vitro experiment

Fluorescence imaging demonstrated that the samples were not harmful to cells, but high nanophosphor concentrations (80ug/ml) caused the cells to cluster. Figure 6 revealed small grains of YAG:Ce^{3+} in the sample extracts, which could be linked to integrin-mediated cell adhesion and signaling [13]. The Optic Microscope images (Figure 6) displayed that hFOB-cells firmly adhered to fibers where the nanophosphor crystals acted as anchoring points. Cell labeling showed uniform cell distribution on the scaffold pore surface [14]. All substrates experienced an increase in cell count up to seven generations. Images demonstrated PVA coating supported hFOB cell activity and provided an optimal environment for cell growth [15].

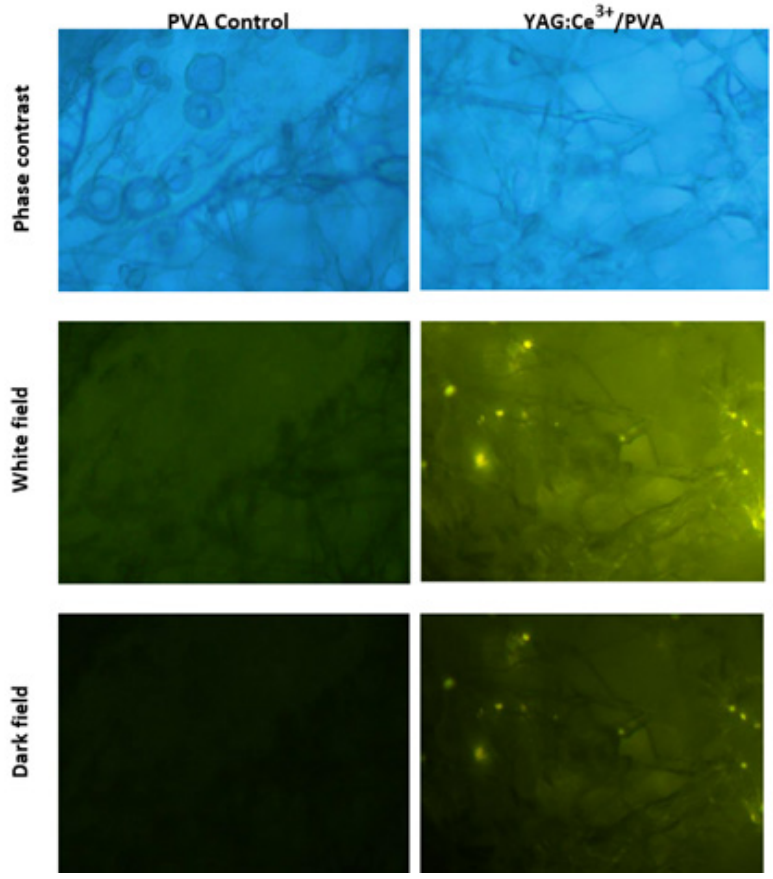

Figure 6: Optical micrographs of human fetal osteoblast (hFOB) cells cultured on PVA/YAG: Ce^{3+} fibers for 7 days at a concentration of 80µg/mL (scale bar=20µm). The optical micrographs illustrate the uniform distribution of cells on the scaffold pore surface, highlighting the scaffold's biocompatibility and potential for bone tissue regeneration.

In contrast to films, the morphology of fibrous scaffolds is well known for its capacity to provide plenty of room for cell adhesion and growth. The cells grown on YAG:Ce^{3+}/PVA loaded fibers in this investigation showed identical shape and morphology, showing that the medication or composite materials had no harmful effects on the cells [16]. Previous research indicates that PVA scaffolds experience degradation within the initial 5 days due to strong physical crosslinking. As the incubation period extends, water infiltrates the crystalline structure of PVA, resulting in scaffold dissolution. Comparatively, pure PVA degrades more than its nanocomposites, highlighting how the inclusion of nanofibrils reduces biodegradation by enhancing physical cross-link density and crystallinity [17]. Moreover, the mechanical properties of nanoparticles, such as their elasticity and deformability, play a crucial role in influencing phagocytosis efficiency and blood circulation time [18]. In fact, macrophages have shown a preference for rigid particles over their softer counterparts, further emphasizing the importance of considering the impact of nanoparticles' mechanical characteristics on their performance. These findings will be included in ongoing viability tests.

Animal study results

In Figure 7, optical micrographs illustrate the control PVA and YAG:Ce^{3+}/PVA (10%w/v) composites after their implantation into the backs of adult male Wistar rats for 2 and 4 weeks. The results demonstrate successful integration of the implants with the surrounding collagen fibers. After twenty days of in vivo implantation, degradation of the implants was observed, with intertwining occurring within the newly formed extracellular matrix as part of the tissue repair process. Mild to moderate

inflammatory reactions were observed in all groups, characterized by the presence of eosinophils, neutrophils, and macrophages. Furthermore, at the 4-week mark, a thin layer of host cell infiltration was visible on the implant's surface, indicating a favorable host response to the YAG:Ce^{3+}/PVA tracking composites. It can be observed that during the first week, there was a higher influx of eosinophils and histiocytes. As the experiment progressed, reaching its culmination, the granuloma formed in the early days appeared to be restrictive. Blood vessels and nerves were observed without any damage, meeting the established parameters for implant rejection determination. It is worth noting that in all cases, large multinucleated FBGCs (arrows) and degrading polymer were observed. However, at 2 weeks, the uncoated portion of the scaffolds elicited a robust FBGC response. Numerous FBGCs were seen in dense collagenous tissue adjacent to the degrading polymer, lining the interface between tissue and polymer. By 4 weeks, the uncoated polymer had undergone extensive degradation, resulting in polymer fragmentation at multiple sites, each surrounded by multiple FBGCs [19].

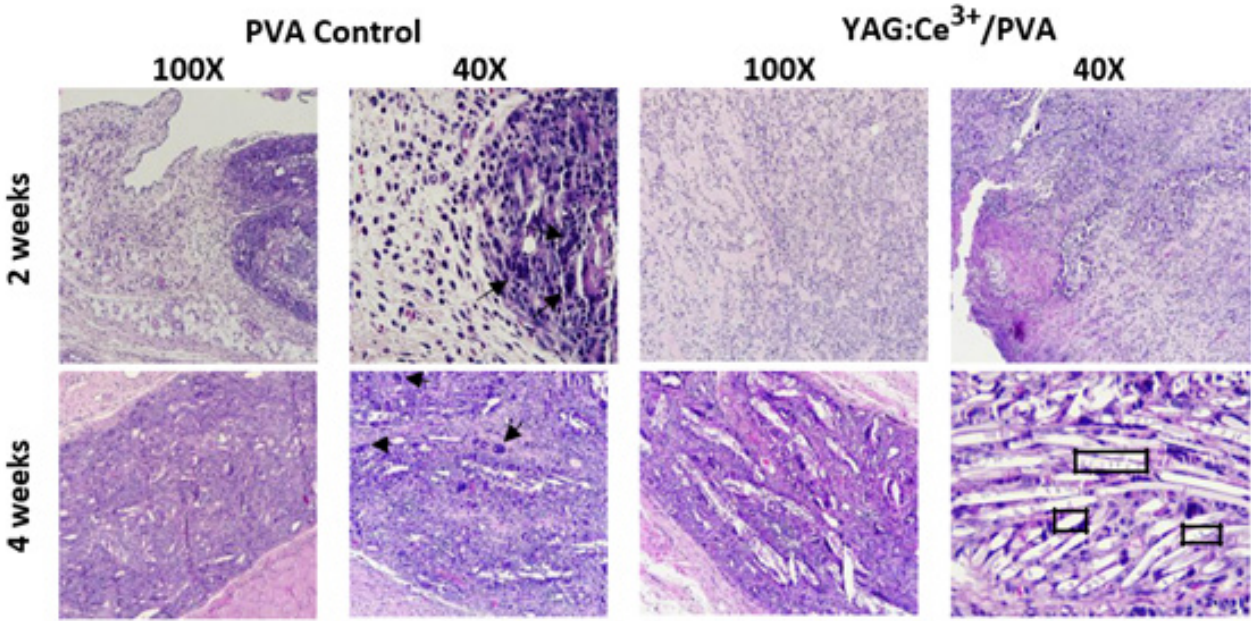

Figure 7: Optical micrographs of control PVA and YAG:Ce^{3+}/PVA (10%w/v) after implantation into the back of adult male Wistar rats at the indicated points (2 and 4 weeks). The photomicrographs stained with H&E demonstrate close integration of the implants with the surrounding collagen fiber. Additionally, after 20 days of implantation, partial degradation of the implants is observed (squares). The inflammatory reactions in all groups were mild to moderate, with no significant differences at 28 days after surgery (100X and 40X).

Conclusion

Our study successfully produced sol-gel YAG:Ce_{3+} nanophosphors with an average size of 65nm. Air-jet spraying was used to generate the PVA/ YAG:Ce^{3+} composite scaffold, resulting in fibers with a random distribution and an average diameter of up to 400nm. The scaffold produced a luminous yellow light when exposed to 450nm radiation, demonstrating the nanophosphors' outstanding photo stability and lack of quenching effects. Regarding biocompatibility, the cellular attachment of the osteoblasts was unaffected by the PVA/YAG:Ce^{3+} fiber nanocomposite. The nanocomposite improved healthy cell functionality at an 80ug/ml concentration by supplying a microenvironment linked to the nanometric interconnectivity of the fiber scaffold, as indicated by the mineral-like deposit. YAG:Ce_{3+}/ PVA scaffolds demonstrated a significant ability to promote the growth of osteoblast hFOB cells. Additionally, after 8 weeks, the polymer-conjugated scaffold underwent extensive degradation, leading to the fragmentation of the polymer at various locations, with each site surrounded by multiple FBGCs. Further studies can focus on the scaffold's structural-biological features to gain more insights into its suitability for long term tracking composites for bone tissue regeneration.

Funding

The authors are grateful for the financial support of the DGAPA-UNAM: PAPIIT IN213821 project and the CONACYT by the particular program of Fondo Sectorial de Investigación para la Educación A1-S-9178 project.

Data Availability Statement

All data generated for this study are included in the manuscript.

Acknowledgments

We appreciate the support provided by the CONACYT through its scholarship (number: 613415 and CVU: 745379) to Rodrigo Osorio Arciniega during his Doctoral studies in the Programa de

Maestría y Doctorado en Ciencias Médicas, Odontológicas y de la Salud at UNAM. The authors want to thank Raul Reyes Ortíz and Adriana Tejeda Cruz from IIM-UNAM for their technical assistance and support.

Conflicts of Interest

The authors declare that the research was conducted without any commercial or financial relationships that could be construed as a potential conflict of interest.

References

1. Balaram V (2019) Rare earth elements: A review of applications, occurrence, exploration, analysis, recycling, and environmental impact. Geosci Front 10(4): 1285-1303.
2. Natarajan D, Ye Z, Wang L, Ge L, Pathak JL (2022) Rare earth smart nanomaterials for bone tissue engineering and implantology: Advances, challenges, and prospects. Bioengineering & Translational Medicine 7(1): e10262.
3. Li X, Chen H (2016) Yb^{3+}/Ho^{3+} co-doped apatite upconversion nanoparticles to distinguish implanted material from bone tissue. ACS Applied Materials & Interfaces 8(41): 27458-27464.
4. Chaudhuri B, Mondal B, Ray SK, Sarkar SC (2016) A novel biocompatible conducting polyvinyl alcohol (PVA)-polyvinylpyrrolidone (PVP)-hydroxyapatite (HAP) composite scaffolds for probable biological application. Colloids and surfaces B: Biointerfaces 143: 71-80.
5. Zhang Y, Qiao X, Wan J, Wu LA, Chen B, et al. (2017) Facile synthesis of monodisperse YAG: Ce^{3+} microspheres with high quantum yield via an epoxide-driven sol-gel route. Journal of Materials Chemistry C 5(35): 8952-8957.
6. Gash AE, Tillotson TM, Satcher Jr JH, Hrubesh LW, Simpson RL (2001) New sol-gel synthetic route to transition and main-group metal oxide aerogels using inorganic salt precursors. Journal of Non-Crystalline Solids 285(1-3): 22-28.
7. Hu S, Liu Y, Zhang Y, Xue Z, Wang Z, et al. (2019) 3D printed ceramic phosphor and the photoluminescence property under blue laser excitation. Journal of the European Ceramic Society 39(8): 2731-2738.
8. Zhang Y, Qiao X, Wan J, Wu LA, Chen B, et al. (2017) Facile synthesis of monodisperse YAG: Ce^{3+} microspheres with high quantum yield via an epoxide-driven sol–gel route. Journal of Materials Chemistry C 5(35): 8952-8957.
9. Wang Z, Xu M, Zhang W, Yin M (2007) Synthesis and luminescent properties of nano-scale LuAG: RE^{3+} (Ce, Eu) phosphors prepared by co-precipitation method. Journal of luminescence 122-123: 437-439.
10. Gai S, Li C, Yang P, Lin J (2014) Recent progress in rare earth micro/nanocrystals: Soft chemical synthesis, luminescent properties, and biomedical applications. Chemical Reviews 114(4): 2343-2389.
11. Meng D, Lei X, Li Y, Kong Y, Huang D, et al. (2020) Three dimensional polyvinyl alcohol scaffolds modified with collagen for $HepG_2$ cell culture. Journal of Biomaterials Applications 35(4-5): 459-470.
12. Mahalingam S, Bayram C, Gultekinoglu M, Ulubayram K, Homer-Vanniasinkam S, et al. (2021) Co-Axial gyro-spinning of PCL/PVA/HA core-sheath fibrous scaffolds for bone tissue engineering. Macromolecular Bioscience 21(10): 2100177.
13. Kim K, Dean D, Lu A, Mikos AG, Fisher JP (2011) Early osteogenic signal expression of rat bone marrow stromal cells is influenced by both hydroxyapatite nanoparticle content and initial cell seeding density in biodegradable nanocomposite scaffolds. Acta Biomaterialia 7(3): 1249-1264.
14. Osorio AR, García HM, Alvarez FO, Alvarez Perez MA (2021) Composite fiber spun mat synthesis and in vitro biocompatibility for guide tissue engineering. Molecules 26(24): 7597.
15. Shokrgozar MA, Bonakdar S, Dehghan MM, Hojjati Emami S, Montazeri L, et al. (2013) Biological evaluation of polyvinyl alcohol hydrogel crosslinked by polyurethane chain for cartilage tissue engineering in rabbit model. Journal of Materials Science: Materials in Medicine 24(10): 2449-2460.
16. Yar M, Farooq A, Shahzadi L, Khan AS, Mahmood, et al. (2016) Novel meloxicam releasing electrospun polymer/ceramic reinforced biodegradable membranes for periodontal regeneration applications. Materials Science and Engineering C64: 148-156.
17. Enayati MS, Behzad T, Sajkiewicz P, Rafienia M, Bagheri R, et al. (2018) Development of electrospun poly (vinyl alcohol)-based bionanocomposite scaffolds for bone tissue engineering. Journal of Biomedical Materials Research Part A 106(4): 1111-1120.
18. Zhang YN, Poon W, Tavares AJ, McGilvray ID, Chan WCW (2016) Nanoparticle-liver interactions: Cellular uptake and hepatobiliary elimination. Journal of Controlled Release 240: 332-348.
19. Lickorish D, Chan J, Song J, Davies JE (2004) An in-vivo model to interrogate the transition from acute to chronic inflammation. Eur Cell Mater 8: 12-19.